

# CH<sup>+</sup>(1-0) and <sup>13</sup>CH<sup>+</sup>(1-0) absorption lines in the direction of massive star-forming regions<sup>\*</sup>

E. Falgarone<sup>1</sup>, B. Godard<sup>8,1</sup>, J. Cernicharo<sup>3</sup>, M. De Luca<sup>1</sup>, M. Gerin<sup>1</sup>, T. G. Phillips<sup>7</sup>, J. H. Black<sup>2</sup>, D. C. Lis<sup>7</sup>, T. A. Bell<sup>7</sup>, F. Boulanger<sup>8</sup>, A. Coutens<sup>12,13</sup>, E. Dartois<sup>8</sup>, P. Encrenaz<sup>1</sup>, T. Giesen<sup>9</sup>, J. R. Goicoechea<sup>3</sup>, P. F. Goldsmith<sup>6</sup>, H. Gupta<sup>6</sup>, C. Gry<sup>10</sup>, P. Hennebelle<sup>1</sup>, E. Herbst<sup>4</sup>, P. Hily-Blant<sup>11</sup>, C. Joblin<sup>12,13</sup>, M. Kaźmierczak<sup>15</sup>, R. Kołos<sup>14</sup>, J. Krelowski<sup>15</sup>, J. Martin-Pintado<sup>3</sup>, R. Monje<sup>7</sup>, B. Mookerjee<sup>15</sup>, D. A. Neufeld<sup>5</sup>, M. Perault<sup>1</sup>, J. C. Pearson<sup>6</sup>, C. Persson<sup>2</sup>, R. Plume<sup>16</sup>, M. Salez<sup>1</sup>, M. Schmidt<sup>18</sup>, P. Sonnentrucker<sup>5</sup>, J. Stutzki<sup>9</sup>, D. Teyssier<sup>19</sup>, C. Vastel<sup>12,13</sup>, S. Yu<sup>6</sup>, K. Menten<sup>21</sup>, T. R. Geballe<sup>22</sup>, S. Schlemmer<sup>9</sup>, R. Shipman<sup>23</sup>, A.G.G.M. Tielens<sup>24</sup>, S. Philipp<sup>25</sup>, A. Cros<sup>12,13</sup>, J. Zmuidzinas<sup>7</sup>, L.A. Samoska<sup>6</sup>, K. Klein<sup>26</sup>, A. Lorenzani<sup>27</sup>, R. Szczerba<sup>18</sup>, I. Péron<sup>28,1</sup>, P. Cais<sup>29</sup>, P. Gaufre<sup>29</sup>, A. Cros<sup>12,13</sup>, L. Ravera<sup>12,13</sup>, P. Morris<sup>30</sup>, S. Lord<sup>30</sup>, P. Planesas<sup>31,32</sup>

(Affiliations can be found after the references)

Received / Accepted

## ABSTRACT

We report the detection of the ground-state rotational transition of the methylidyne cation CH<sup>+</sup> and its isotopologue <sup>13</sup>CH<sup>+</sup> toward the remote massive star-forming regions W33A, W49N, and W51 with the HIFI instrument onboard the *Herschel* satellite. Both lines are seen only in absorption against the dust continuum emission of the star-forming regions. The CH<sup>+</sup> absorption is saturated over almost the entire velocity ranges sampled by the lines-of-sight that include gas associated with the star-forming regions (SFR) and Galactic foreground material. The CH<sup>+</sup> column densities are inferred from the optically thin components. A lower limit of the isotopic ratio [<sup>12</sup>CH<sup>+</sup>]/[<sup>13</sup>CH<sup>+</sup>] > 35.5 is derived from the absorptions of foreground material toward W49N. The column density ratio,  $N(\text{CH}^+)/N(\text{HCO}^+)$ , is found to vary by at least a factor 10, between 4 and > 40, in the Galactic foreground material. Line-of-sight <sup>12</sup>CH<sup>+</sup> average abundances relative to total hydrogen are estimated. Their average value,  $N(\text{CH}^+)/N_{\text{H}} > 2.6 \times 10^{-8}$ , is higher than that observed in the solar neighborhood and confirms the high abundances of CH<sup>+</sup> in the Galactic interstellar medium. We compare this result to the predictions of turbulent dissipation regions (TDR) models and find that these high abundances can be reproduced for the inner Galaxy conditions. It is remarkable that the range of predicted  $N(\text{CH}^+)/N(\text{HCO}^+)$  ratios, from 1 to ~ 50, is comparable to that observed.

**Key words.** Astrochemistry - ISM : molecules - ISM : kinematics and dynamics - Turbulence

## 1. Introduction

The methylidyne ion CH<sup>+</sup> was among the first molecules to be detected in the interstellar medium (ISM) Douglas & Herzberg (1941). For decades, CH<sup>+</sup> remained accessible only in absorption at 423.2 nm, restricting its investigation to the lines-of-sight (*los*) toward bright nearby stars. The CH<sup>+</sup> abundances observed in the local diffuse ISM are several orders of magnitude above the predictions of UV-driven steady-state models (see references in Godard et al. 2009), raising one of the most intractable puzzles in our understanding of the ISM. Unfortunately, the detection of the CH<sup>+</sup> ground-state rotational transition has been prevented for a long time for two independent reasons. CH<sup>+</sup> being a light molecule, its lowest rotational transition lies in the submillimetre range. Its high reactivity makes it difficult to isolate in laboratory experiments (Pearson & Drouin 2006). Only recently did successful experiments provide accurate frequency determinations (Amano 2010). Moreover, ground-based astronomical detection of <sup>12</sup>CH<sup>+</sup>(1-0) is prevented by its proximity to a strong atmospheric line of water vapor. The first detection of the CH<sup>+</sup> rotational lines (above  $J=2-1$ ) was achieved by *ISO-LWS* in the plan-

etary nebula NGC7027 (Cernicharo et al. 1997). The CH<sup>+</sup>(1-0) line has now been detected in emission and absorption with the *Herschel*/HIFI instrument (Pilbratt et al. 2010; de Graauw et al. 2010) in DR21 (Falgarone et al. 2010) and, as spectrally unresolved lines with the *Herschel*/SPIRE FTS (Griffin et al. 2010), in emission in the Orion Bar and in absorption in two SFRs (Naylor et al. 2010). The ground-state transition of the isotopologue <sup>13</sup>CH<sup>+</sup>, at a frequency lower by ~ 5 GHz, can be observed under exceptional atmospheric conditions and was detected in absorption toward SgrB2(M) and several massive SFRs of the inner Galaxy with the Atacama Pathfinder Experiment (APEX) telescope (Menten et al. 2010) and the Caltech Submillimeter Observatory (CSO) telescope (Falgarone et al. 2005, Falgarone et al. in prep.).

In this *Letter*, we report the detection of the <sup>12</sup>CH<sup>+</sup> and <sup>13</sup>CH<sup>+</sup> transitions toward the massive SFRs W33A, W49N, and W51. The HIFI observations are described in Sect. 2. The results, given in Sect. 3, are compared to models in Sect. 4.

## 2. HIFI observations and data reduction

The observations presented here were carried out on 2010 April 13 with the *Herschel*/HIFI instrument in the framework of the key programme PRISMAS. We observed the  $J = 1 - 0$  transi-

<sup>\*</sup> *Herschel* is an ESA space observatory with science instruments provided by European-led Principal Investigator consortia and with important participation from NASA.

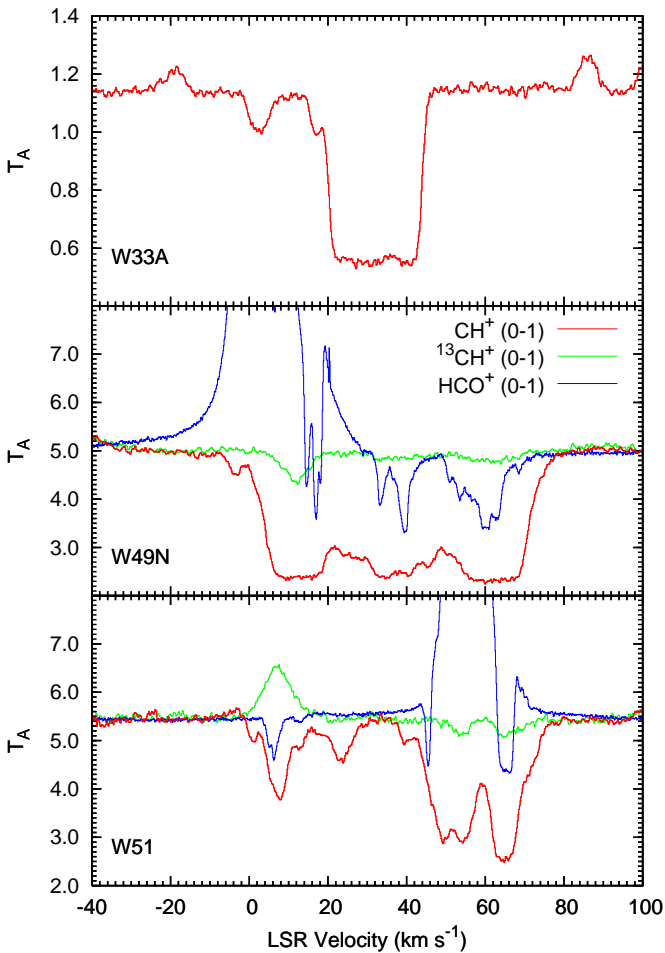


**Fig. 1.**  $\text{CH}^+$  (1-0) and  $^{13}\text{CH}^+$  (1-0) *Herschel*/HIFI spectra, and  $\text{HCO}^+$  (1-0) IRAM-30m spectra observed toward W33A ( $\text{CH}^+$  only), W49N, and W51. The  $\text{CH}^+$  and  $^{13}\text{CH}^+$  (1-0) spectra are shown assuming rest frequencies of 835 137 MHz and 830 215 MHz respectively. Toward W49N and W51, the  $\text{HCO}^+$  (1-0) spectra are shifted by 3.2 and 4.4 K respectively, to match the observed  $\text{CH}^+$  continuum levels. Note that since the DBS mode is used, any absorption line profile deeper than one-half the continuum level suggests a sideband gain ratio which differs from unity. Emission lines in the  $\text{CH}^+$  and  $^{13}\text{CH}^+$  spectra are all methanol lines from the SFRs.

tions of  $\text{CH}^+$  and  $^{13}\text{CH}^+$ , with rest frequencies of 835.1375 and 830.2150 GHz (Amano 2010), in the upper and lower sidebands of the Band 3a HIFI receiver respectively, using the dual beam switch (DBS) mode and the wide band spectrometer (WBS) with a frequency resolution of 1.1 MHz. In these frequency ranges, the corresponding velocity resolution is  $\sim 0.36 \text{ km s}^{-1}$ , and the *Herschel* HPBW at 835.1 GHz is  $26''$ . The FIR background continuum sources observed were three remote massive star-forming regions in the Galactic plane, W33A, W49N, and W51 (distances from the Sun : 4, 11.5 and 7 kpc respectively) at central positions of  $\alpha = 18\text{h } 14\text{m } 39.4\text{s}$ ,  $\delta = -17^\circ 52' 00''$ ,  $\alpha = 19\text{h } 10\text{m } 13.2\text{s}$ ,  $\delta = +09^\circ 06' 12''$ , and  $\alpha = 19\text{h } 23\text{m } 43.9\text{s}$ ,  $\delta = +14^\circ 30' 30.5''$  (J2000) respectively.

The data were reduced using the standard *Herschel* pipeline to Level 2, providing fully calibrated spectra, subsequently analysed using the GILDAS-CLASS90 software<sup>1</sup> (Hily-Blant et al.

<sup>1</sup> See <http://www.iram.fr/IRAMFR/GILDAS> for more information about the GILDAS softwares.

2005). The average spectra displayed in Fig. 1 as functions of the local standard of rest (LSR) velocity were obtained by combining the data from three observations with different settings of the local oscillator frequency (carried out to separate the lines originating from the upper and lower sidebands) and from both polarizations. For comparison, we also display the  $J = 1 - 0$  lines of  $\text{HCO}^+$  observed at the IRAM-30m telescope by Godard et al. (2010).

Thanks to the saturated shape of the  $\text{CH}^+$  absorption line profiles, we measured the sideband gain ratios  $R$  at 835.1375 GHz, defined as the ratio of the continuum temperatures measured in the lower and upper sidebands. For all the spectra with saturated absorption lines, we found  $R \sim 1$  and  $R \sim 0.8$  in the horizontal and vertical polarization respectively. Since we are interested in the velocity structure and the properties of the absorbing gas, the spectra in both polarizations were normalized to their respective continuum temperature and then averaged (Fig. 2).

These spectra exhibit a few remarkable properties: (1) there is no emission line detected at the velocities of the SFRs (see Table 1), unlike what has been observed in the direction of DR21 (Falgarone et al. 2010) and the Orion Bar (Naylor et al. 2010), (2)  $\text{CH}^+$  absorption covers almost all velocities sampled by the  $l_{\text{os}}$ , and (3) several velocity components, unseen in  $\text{HCO}^+$  are detected in  $\text{CH}^+$ , for instance at LSR velocities  $23.4 \text{ km s}^{-1}$  and  $40 \text{ km s}^{-1}$  on the W51  $l_{\text{os}}$ , the former being also detected in absorption in  $\text{HF}(1-0)$  (Sonnentrucker et al. 2010) and  $\text{H}_2\text{O}^+$  (Wyrowski et al. 2010).

### 3. Line profiles analysis and results

The spectra have been decomposed into individual velocity components and the column densities of  $\text{CH}^+$  and  $^{13}\text{CH}^+$  were inferred from a multi-Gaussian fitting procedure based on the Levenberg-Marquardt algorithm and developed by Godard et al. (2010). To correctly determine the opacity of weak absorption features blended with saturated lines, we applied an empirical model to account for the  $\text{CH}^+$  saturated line profiles (see magenta profiles in Fig. 2). All the results are listed in Tables A.1 & A.2 of Appendix A, and shown in Fig. 2.

The column densities of optically thin lines given in the last columns of Tables A.1 & A.2 are derived assuming a low excitation temperature  $T_{\text{ex}} = 3 \text{ K}$  (a valid assumption for the components associated with the diffuse gas along the  $l_{\text{os}}$ ):  $N(\text{CH}^+) = 3.11 \times 10^{12} \int \tau dv \text{ cm}^{-2}$  and  $N(^{13}\text{CH}^+) = 3.05 \times 10^{12} \int \tau dv \text{ cm}^{-2}$ . However, these relations set a lower limit for the velocity components associated with the SFR where  $T_{\text{ex}}$  is likely higher: for  $T_{\text{ex}} = 40 \text{ K}$ , the corresponding scaling factors are about twice as large. Finally, for the saturated  $\text{CH}^+$  features, lower limits on the column densities are inferred assuming a conservative lower limit on the optical depth of 2.3 (Neufeld et al. 2010). The uncertainties given in Tables 1, A.1 & A.2 are the formal  $1-\sigma$  errors derived from the diagonal elements of the covariance matrix and do not take into account the systematic errors introduced by the uncertainty in the continuum level  $T_c$  and by the dependence of the Gaussian decomposition on the input parameters. An uncertainty  $\delta T_c/T_c$  of 10 % induces an error on the derived column density which ranges from 3 % to 62 % when the central optical depth  $\tau_0$  varies between 0.1 and 2.

We find that the distribution of the FWHM (full width at half maximum) of the  $\text{CH}^+$  velocity components is continuous between 2.2 and  $8.4 \text{ km s}^{-1}$ . The signal/noise ratio of the  $^{13}\text{CH}^+$  spectra is not sufficient to allow the identification of narrow components. As a result, the FWHMs of the  $^{13}\text{CH}^+$  line profiles are

**Table 1.** CH<sup>+</sup> (0 – 1) and <sup>13</sup>CH<sup>+</sup> (0 – 1) absorption lines analysis. The column densities are derived assuming an excitation temperature  $T_{\text{ex}} = 3$  K.

source	velocity component	$u_{\text{min}}$ km s <sup>-1</sup>	$u_{\text{max}}$ km s <sup>-1</sup>	$N(\text{CH}^+)$ 10 <sup>13</sup> cm <sup>-2</sup>	$N(^{13}\text{CH}^+)$ 10 <sup>12</sup> cm <sup>-2</sup>	$50 \times N(^{13}\text{CH}^+)$ 10 <sup>13</sup> cm <sup>-2</sup>	$N(\text{HCO}^+)^a$ 10 <sup>12</sup> cm <sup>-2</sup>	$\frac{N(\text{CH}^+)}{N(\text{HCO}^+)}$	$N_{\text{H}}^b$ 10 <sup>22</sup> cm <sup>-2</sup>
W33A	star forming region	19	60	> 16.7	–	–	–	–	–
	foreground	–4	19	0.8 ± 0.1	–	–	–	–	0.8 ± 0.4
W49N	star forming region	–20	30	> 16.6	> 6.7	> 33.5	–	–	–
	foreground	30	80	> 27.7	7.8 ± 0.6	39 ± 3	25 ± 1	> 11	4.1 ± 0.4
W51	star forming region	43	80	> 12.8	> 5.4	> 27.0	–	–	–
	foreground	15	43	1.0 ± 0.1	–	–	< 0.25	> 40	2.5 ± 0.6
	foreground	–2	15	1.7 ± 0.1	–	–	4.1 ± 0.4	4	–

<sup>a</sup> From Godard et al. (2010).

<sup>b</sup> From models of the extinction at 2 μm by Marshall et al. (2006).

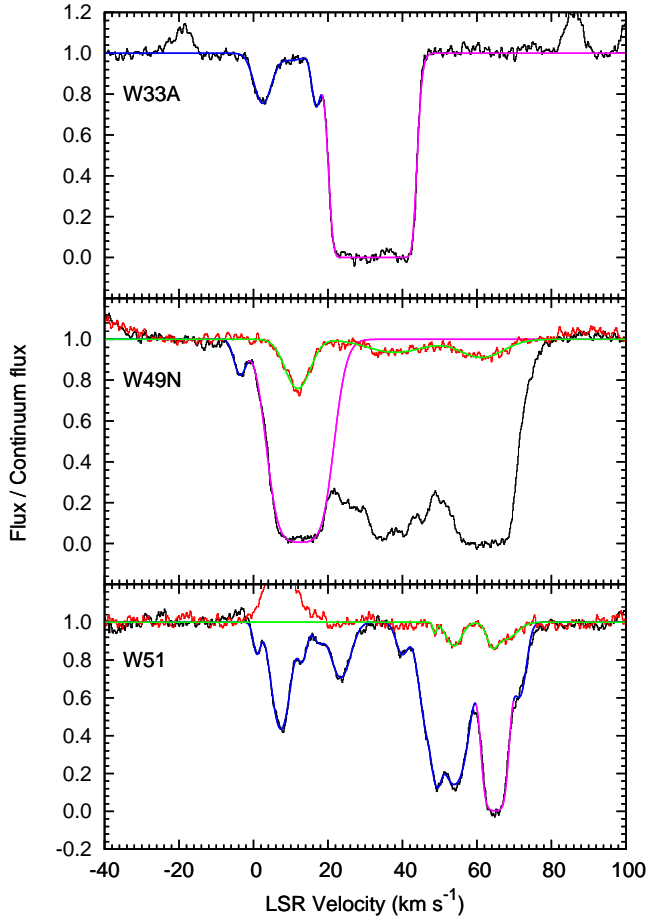


**Fig. 2.** Superimposition of the CH<sup>+</sup> (black) and <sup>13</sup>CH<sup>+</sup> (red) spectra observed toward W33A (top panel), W49N (middle panel) and W51 (bottom panel). The observational points are compared to empirical models (magenta line) of saturated line profiles, and to the results of the multi-Gaussian decomposition of the CH<sup>+</sup> (blue line) and the <sup>13</sup>CH<sup>+</sup> (green line) absorption spectra.

large (up to 18 km s<sup>-1</sup>). Lastly, the CH<sup>+</sup> column densities *per velocity component* are found to range between 10<sup>12</sup> cm<sup>-2</sup> and 1.7 × 10<sup>14</sup> cm<sup>-2</sup>, a range very similar to that obtained in the local ISM (Crane et al. 1995, Gredel 1997, Weselak et al. 2008). It is

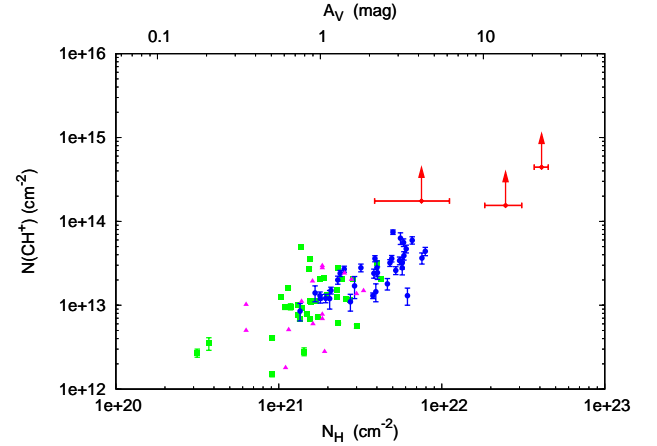


**Fig. 3.** Dependence of CH<sup>+</sup> column densities on the total hydrogen column density  $N_{\text{H}} = N(\text{H}) + 2N(\text{H}_2)$ . The values obtained for the *los* toward W33A, W49N, and W51 are lower limits (red rhombus). The values derived from absorption lines at 423.2 nm are from Crane et al. (1995) (magenta triangles), Gredel (1997) (blue dots) and Weselak et al. (2008) (green squares). Note that the  $N(\text{CH}^+)/N_{\text{H}}$  values obtained along the inner Galaxy *los* (submillimetre data) are larger than the mean value observed in the local ISM.

interesting that in either sample, the smallest CH<sup>+</sup> linewidths and column densities are so similar ( $\sim 2$  km s<sup>-1</sup> and  $\sim 10^{12}$  cm<sup>-2</sup>), while the resolving power of the submillimetre and visible observations are so different.

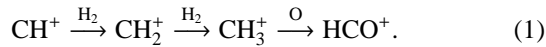
The results for the each *los* are summarized in Table 1 where we have separated the absorption components in the velocity range of the star-forming regions from those originating in unrelated Galactic foreground gas. The <sup>13</sup>CH<sup>+</sup> and <sup>12</sup>CH<sup>+</sup> column densities of the foreground gas on the W49N *los* provide a lower limit of the isotopic ratio  $[\text{CH}^+]/[\text{CH}^+] > 35.5$ , consistent with the results of Casassus et al. (2005); Stahl et al. (2008). Three  $N(\text{CH}^+)/N(\text{HCO}^+)$  ratios, computed using the observed  $N(\text{HCO}^+)$  values of Godard et al. (2010), are found to be scattered by more than a factor 10. Note that the 23.4 km s<sup>-1</sup> CH<sup>+</sup> component on the W51 *los* is barely visible in the HCO<sup>+</sup>(1-0) profile. In that case, the abundance ratio cannot be determined properly because of the broad HCO<sup>+</sup> line wing.

The CH<sup>+</sup> column densities integrated along the *los* are displayed as a function of the extinction (or total hydrogen column density,  $N_{\text{H}} = N(\text{H}) + 2N(\text{H}_2)$ ) along each *los* (Fig. 3) to allow for a com-

parison with the local ISM values. The comparison with  $N(\text{H}_2)$  will be carried out using the PRISMAS CH column densities along the same *los* as tracers of  $N(\text{H}_2)$  (Gerin et al. 2010). The average of the inner Galaxy values,  $N(\text{CH}^+)/N_{\text{H}} > 2.6 \times 10^{-8}$ , is higher than the local ISM average,  $N(\text{CH}^+)/N_{\text{H}} = 8 \times 10^{-9}$ . We note, however, the large scatter of the local ISM values. Moreover, for the inner Galaxy *los*,  $N_{\text{H}}$  is inferred from K extinction measurements at a resolution of  $0.25^\circ$  (Marshall et al. 2006) which possibly underestimates the true column density over which the  $\text{CH}^+$  absorption occurs, in particular the pc-scale envelope of the SFRs. We need  $\text{CH}^+(2-1)$  data (included in the PRISMAS programme) to disentangle  $\text{CH}^+$  absorption in diffuse extended gas from that arising in the environment of the SFRs.

#### 4. Comparison with model predictions

The large observed abundances of  $\text{CH}^+$  have always been a major puzzle of the diffuse interstellar chemistry, since the only reaction efficient enough to form this molecular ion,  $\text{C}^+ + \text{H}_2 \rightarrow \text{CH}^+ + \text{H}$ , is highly endothermic ( $E/k = 4640$  K). This suggests that large amounts of suprathermal energy are deposited in the cold neutral medium. In the past, several scenarios have been investigated, including C-shocks (Pineau des Forêts et al. 1986), turbulent interfaces between the warm and cold neutral medium (Lesaffre et al. 2007), and regions of intermittent turbulent dissipation (TDR models, Godard et al. 2009). While the reaction between  $\text{C}^+$  and vibrationally excited  $\text{H}_2$  could account for the large  $\text{CH}^+$  abundances in dense and highly illuminated photodissociation regions (PDR), this mechanism is found inefficient for the physical conditions of the diffuse ISM (Sternberg & Dalgarno 1995; Agundez et al. 2010). This riddle could be related to the observed excess of  $\text{HCO}^+$  in the diffuse ISM (see references in Godard et al. 2010) because  $\text{CH}^+$ -rich environments with  $\text{H}_2$  molecular fractions as low as 25% enhance the production of  $\text{HCO}^+$  through the ion-neutral reaction chain



The TDR code is a 1-dimensional model in which the chemical and thermal evolution of a turbulent dissipative burst - namely a magnetized vortex - is computed. The lifetime of the burst is controlled by the turbulent rate-of-strain  $a$  of the large scales. At any time, a large number of these tiny regions ( $\sim 100$  AU), altogether filling a small fraction of the entire *los*, are developing a transient warm chemistry triggered by both the viscous dissipation and the ion-neutral friction, where local  $\text{CH}^+$  and  $\text{HCO}^+$  abundances reach  $10^{-6}$  and  $3 \times 10^{-7}$  respectively (Godard et al. 2009). A random *los* therefore samples three kinds of diffuse gas: (1) mainly the ambient medium in which the chemistry is driven by the UV radiation field, (2) the active vortices with a filling factor set by the energy transfer rate in the turbulent cascade,  $\epsilon = \rho v_l^3/l$ , identified with the turbulent dissipation rate (here,  $v_l$  is the characteristic velocity at scale  $l$ ), and (3) the long-lasting relaxation stages where the gas previously heated cools down to its original state.

The resulting average abundance is found to scale as  $N(\text{CH}^+)/N_{\text{H}} = 6.4 \times 10^{-8} (\epsilon/\epsilon_0) (n_{\text{H}}/50 \text{ cm}^{-3})^{-2.6} (A_V/0.4)^{-1}$  for an ambient radiation field  $\chi = 3$  in ISRF units, and  $\epsilon_0 = 2 \times 10^{-24} \text{ erg cm}^{-3} \text{ s}^{-1}$ , two values representative of the inner Galaxy conditions. This scaling holds for gas densities  $30 \text{ cm}^{-3} \leq n_{\text{H}} \leq 500 \text{ cm}^{-3}$ , visual extinctions from the ISRF  $0.2 < A_V < 1$  and a rate-of-strain  $a = 10^{-11} \text{ s}^{-1}$  close to observed values (Falgarone et al. 2009). The predicted  $\text{CH}^+$  abundances are therefore in excellent agreement with the average observed lower limits in the

inner Galaxy, for  $n_{\text{H}} \leq 75 \text{ cm}^{-3}$  ( $\epsilon/\epsilon_0$ ) $^{0.38} (A_V/0.4)^{-0.38}$ . In the TDR model, the  $\text{CH}^+$  and  $\text{HCO}^+$  abundances are strongly dependent on  $n_{\text{H}}$  but, interestingly, their ratio only depends on the relaxation times set by  $a$ . For  $10^{-12} \text{ s}^{-1} \leq a \leq 10^{-9} \text{ s}^{-1}$ ,  $N(\text{CH}^+)/N(\text{HCO}^+)$  increases between 1 and 50, a result that compares very well with the observations.

#### 5. Conclusion

The *Herschel*/HIFI  $\text{CH}^+(1-0)$  and  $^{13}\text{CH}^+(1-0)$  observations carried out in the framework of the PRISMAS key-programme in the direction of the remote massive star-forming regions W33A, W49N, and W51 provide several new results. Unlike in DR21, both lines are detected only in absorption. The  $\text{CH}^+$  absorption is saturated over broad velocity intervals and unlike  $\text{HCO}^+$ , is detected at all the velocities sampled by the *los*, including those of the star-forming regions. A lower limit of the isotopic ratio  $[^{12}\text{CH}^+]/[^{13}\text{CH}^+] > 35.5$  is obtained. The column density ratio,  $N(\text{CH}^+)/N(\text{HCO}^+)$  is found to vary between 4 and  $> 40$ , among the foreground velocity components. Line-of-sight  $^{12}\text{CH}^+$  abundances relative to total hydrogen are estimated. Their average,  $N(\text{CH}^+)/N_{\text{H}} > 2.6 \times 10^{-8}$ , is larger than that the local ISM and confirms the high abundances of  $\text{CH}^+$  in the Galactic interstellar medium. Both the high  $\text{CH}^+$  abundances and the values of the  $N(\text{CH}^+)/N(\text{HCO}^+)$  ratios (and their large scatter) are understood in the framework of models in which chemistry includes routes opened locally by turbulent dissipation bursts (TDR models).

*Acknowledgements.* HIFI has been designed and built by a consortium of institutes and university departments from across Europe, Canada and the United States (NASA) under the leadership of SRON, Netherlands Institute for Space Research, Groningen, The Netherlands, and with major contributions from Germany, France and the US. Consortium members are : Canada: CSA, U. Waterloo; France : CESR, LAB, LERMA, IRAM; Germany : KOSMA, MPIfR, MPS; Ireland : NUI Maynooth; Italy : ASI, IFSI-INAF, Osservatorio Astrofisico di Arcetri-INAF; Netherlands : SRON, TUD; Poland : CAMK, CBK; Spain : Observatorio Astronómico Nacional (IGN), Centro de Astrobiología; Sweden : Chalmers University of Technology - MC2, RSS & GARD, Onsala Space Observatory, Swedish National Space Board, Stockholm University - Stockholm Observatory; Switzerland : ETH Zurich, FHNW; USA : CalTech, JPL, NHSC. MG and EF acknowledge the support from the Centre National de Recherche Spatiale (CNES). DCL is supported by the NSF, award AST-0540882 to the CSO. MS is supported from grant N20339334 from Polish MNiSW.

#### References

- Agundez M., Goicoechea J.R., Cernicharo J. et al. 2010 ApJ 713, 662  
Amano, T. 2010 ApJ 716 L1  
Casassus, S., Stahl, O. & Wilson, T.L. 2005 A&A 441, 181  
Cernicharo J. et al. 1997 ApJL 483 L65  
Crane P., Lambert D.L., Sheffer Y. 1995 ApJS 99 107  
Douglas, A.E., Herzberg, G. 1941 ApJ 94 381.  
Falgarone E., Phillips T.G., Pearson J.C., 2005, ApJ 634, L149.  
Falgarone E., Pety J., Hily-Blant P. 2009 A&A 507, 355  
Falgarone E., Ossenkopf V., Gerin M. et al. 2010 A&A *Herschel* Special Issue  
Flower D. R., Pineau des Forêts G., 1998, MNRAS, 297, 1182 ApJ 392, 602.  
Gerin M. et al. 2010, this volume  
Godard B., Falgarone E., Gerin M., et al. 2010 A&A, in press (arXiv1006.0582)  
Godard B., Falgarone E., Pineau des Forêts G. 2009 A&A 495 847  
Gredel R. 1997 A&A 320, 929  
de Graauw T. et al. 2010, A&A *Herschel* Special Issue  
Griffin et al. 2010, A&A *Herschel* Special Issue  
Hily-Blant P., Pety J., Guilloteau S. 2005, IRAM Technical Report 2005-1  
Lesaffre P., Gerin M., Hennebelle P., 2007, A&A, 469, 949  
Marshall D.J., Robin A.C., Reylé C., et al. 2006 A&A 453, 635  
Menten K.M., Wyrowski F., Belloche A. et al. A&A submitted  
Naylor, D.A., Dartois E., Habart E. et al. A&A in press  
Neufeld D.A., Sonnentrucker P., Phillips T.G. et al. 2010 A&A *Herschel* Special Issue  
Pearson J.C. & Drouin B.J. 2006 ApJ 647, L83  
Pilbratt G. et al. 2010, A&A *Herschel* Special Issue

## Appendix A: Gaussian decomposition and calculation of column densities

---

- <sup>1</sup> LERMA, CNRS, Observatoire de Paris and ENS, France  
e-mail: edith.falgarone@ens.fr
- <sup>2</sup> Chalmers University of Technology, Göteborg, Sweden.
- <sup>3</sup> Centro de Astrobiología, CSIC-INTA, Madrid, Spain.
- <sup>4</sup> Depts. of Physics, Astronomy & Chemistry, Ohio State Univ., USA.
- <sup>5</sup> The Johns Hopkins University, Baltimore, MD 21218, USA
- <sup>6</sup> JPL, California Institute of Technology, Pasadena, USA.
- <sup>7</sup> California Institute of Technology, Pasadena, CA 91125, USA
- <sup>8</sup> Institut d'Astrophysique Spatiale (IAS), Orsay, France.
- <sup>9</sup> I. Physikalisches Institut, University of Cologne, Germany.
- <sup>10</sup> Laboratoire d'Astrophysique de Marseille (LAM), France.
- <sup>11</sup> Laboratoire d'Astrophysique de Grenoble, France.
- <sup>12</sup> CESR, Université Toulouse 3 and CNRS, Toulouse, France
- <sup>13</sup> CNRS ; UMR5187 ; F-31028 Toulouse, France
- <sup>14</sup> Institute of Physical Chemistry, Polish Academy of Sciences,  
Warsaw, Poland
- <sup>15</sup> Nicolaus Copernicus University, Toruń, Poland.
- <sup>16</sup> Tata Institute of Fundamental Research, Mumbai, India.
- <sup>17</sup> Dept. of Physics & Astronomy, University of Calgary, Canada.
- <sup>18</sup> Nicolaus Copernicus Astronomical Center, Poland
- <sup>19</sup> European Space Astronomy Centre, ESA, Madrid, Spain.
- <sup>20</sup> MPI für Extraterrestrische Physik, Garching, Germany.
- <sup>21</sup> MPI für Radioastronomie, Bonn, Germany.
- <sup>22</sup> Gemini telescope, Hilo, Hawaii, USA
- <sup>23</sup> SRON Netherlands Institute for Space Research, Netherlands
- <sup>24</sup> Sterrewacht Leiden, Netherlands
- <sup>25</sup> Deutsches Zentrum für Luft- und Raumfahrt e. V., Raumfahrt-  
Agentur, Bonn, Germany.
- <sup>26</sup> Department of Physics and Astronomy, University of Waterloo,  
Canada
- <sup>27</sup> Osservatorio Astrofisico di Arcetri-INAF- Florence - Italy
- <sup>28</sup> IRAM, 300 rue de la Piscine, St Martin d'Hères, France
- <sup>29</sup> Laboratoire d'Astrophysique de Bordeaux (LAB), France.
- <sup>30</sup> Infrared Processing Analysis Center, California Institute of  
Technology, Pasadena, USA
- <sup>31</sup> Observatorio Astronómico Nacional (IGN), Spain
- <sup>32</sup> Atacama Large Millimeter/Submillimeter Array, Joint ALMA  
Office, Santiago, Chile

**Table A.1.** CH<sup>+</sup> (0 – 1) absorption line analysis results. The column densities are derived assuming an excitation temperature of 3 K, a lower limit for the absorption components detected at velocity intervals corresponding to the source itself. The first part of the table are the results of the multi-Gaussian decomposition procedure. The second part results from the analysis of the spectra over given velocity ranges: for the saturated CH<sup>+</sup> features, lower limits on the column densities are inferred assuming a conservative lower limit on the optical depth of 2.3 (Neufeld et al. 2010).

source	remark <sup>a</sup>	$\nu_0$ (km s <sup>-1</sup> )	$\Delta\nu$ (km s <sup>-1</sup> )	$\tau_0$	$N(\text{CH}^+)$ (10 <sup>12</sup> cm <sup>-2</sup> )
<b>W33A</b>		2.47 ± 0.13	5.18 ± 0.23	0.28 ± 0.01	4.68 ± 0.40
		10.08 ± 1.17	8.38 ± 4.55	0.03 ± 0.01	0.95 ± 0.66
		16.82 ± 0.05	2.56 ± 0.15	0.28 ± 0.01	2.37 ± 0.24
<b>W49N</b>	E	-3.62 ± 0.06	3.63 ± 0.13	0.18 ± 0.01	> 2.1
<b>W51</b>		0.91 ± 0.05	2.21 ± 0.12	0.18 ± 0.01	1.26 ± 0.13
		7.37 ± 0.03	5.13 ± 0.07	0.83 ± 0.01	13.90 ± 0.35
		13.14 ± 0.07	2.73 ± 0.18	0.21 ± 0.01	1.88 ± 0.20
		17.34 ± 0.16	3.41 ± 0.48	0.10 ± 0.01	1.11 ± 0.23
		23.44 ± 0.06	5.83 ± 0.15	0.35 ± 0.01	6.56 ± 0.28
		39.97 ± 0.11	3.76 ± 0.22	0.18 ± 0.01	2.24 ± 0.21
	E	47.16 ± 0.47	5.25 ± 0.55	0.84 ± 0.09	> 14.3
	E	49.32 ± 0.06	2.40 ± 0.27	0.94 ± 0.16	> 7.3
	E	53.97 ± 0.11	7.26 ± 0.15	1.94 ± 0.03	> 45.9
E	71.56 ± 0.03	3.73 ± 0.07	0.48 ± 0.01	> 5.8	
Source	remark	$\nu_{\min}$ (km s <sup>-1</sup> )	$\nu_{\max}$ (km s <sup>-1</sup> )	$\int \tau d\nu$ (km s <sup>-1</sup> )	$N(\text{CH}^+)$ (10 <sup>12</sup> cm <sup>-2</sup> )
<b>W33A</b>	E,S	20.0	45.0	> 53.6	> 166.5
<b>W49N</b>	E,S	0.0	22.0	> 39.3	> 122.2
	E	22.0	30.0	> 13.5	> 41.9
	S	30.0	49.0	> 41.1	> 127.6
	S	49.0	77.5	> 48.1	> 149.5
<b>W51</b>	E,S	60.0	70.0	> 17.7	> 54.9

<sup>a</sup> E = absorption line profile observed in the star-forming region.  $T_{ex}$  may be underestimated, hence the lower limit on  $N(\text{CH}^+)$ . S = saturated line profile.

**Table A.2.** <sup>13</sup>CH<sup>+</sup> (0 – 1) absorption line analysis results.

source	remark <sup>a</sup>	$\nu_0$ (km s <sup>-1</sup> )	$\Delta\nu$ (km s <sup>-1</sup> )	$\tau_0$	$N(^{13}\text{CH}^+)$ (10 <sup>12</sup> cm <sup>-2</sup> )	$N(\text{CH}^+)^b$ (10 <sup>14</sup> cm <sup>-2</sup> )
<b>W49N</b>	E	11.89 ± 0.05	7.46 ± 0.12	0.28 ± 0.01	> 6.7	> 3.35
		38.15 ± 0.31	17.50 ± 0.83	0.07 ± 0.01	3.77 ± 0.30	1.89 ± 0.15
		61.29 ± 0.20	13.49 ± 0.48	0.09 ± 0.01	4.07 ± 0.25	2.04 ± 0.13
<b>W51</b>	E	48.65 ± 0.11	1.05 ± 0.25	0.06 ± 0.01	>0.2	>0.1
	E	53.84 ± 0.10	4.73 ± 0.25	0.13 ± 0.01	>2.0	>1.0
	E	64.10 ± 0.15	3.18 ± 0.63	0.10 ± 0.03	>1.0	>0.5
	E	67.56 ± 0.78	7.09 ± 1.02	0.09 ± 0.01	>2.2	>1.1

<sup>a</sup> E = absorption line profile observed in the star-forming region.  $T_{ex}$  may be underestimated, hence the lower limit on  $N(^{13}\text{CH}^+)$ .

<sup>b</sup> derived from  $N(^{13}\text{CH}^+)$  assuming a <sup>12</sup>CH<sup>+</sup>/<sup>13</sup>CH<sup>+</sup> isotopic ratio of 50.